Structures 37 (2022) 459–468

Contents lists available at ScienceDirect

Structures

journal homepage: www.elsevier.com/locate/structures

Seismic reliability evaluation of steel gabled frames consisting of web-tapered members using joint analysis of hazard and fragility

Mohammad Malekizadeh [a], Nader Fanaie [b,*], Ali Akbar Pirasteh [c]

[a] Department of Civil Engineering, Academic Center for Education, Culture and Research, Khuzestan Branch, Ahvaz, Iran
[b] Department of Civil Engineering, K. N. Toosi University of Technology, Tehran, Iran
[c] Department of Civil Engineering, Faculty of Engineering, Shahid Chamran University of Ahvaz, Ahvaz, Iran

ARTICLE INFO

Keywords:
Steel gabled frames
Seismic reliability
Joint analysis of hazard and fragility
Annual rate of exceedance

ABSTRACT

Despite the wide application of steel gabled frame (SGF) systems in large industrial projects, the current literature lacks accurate information on their seismic performance to ensure satisfactory performance at different levels of earthquake intensity. Also, given the scant information on the structural performance and their seismic design parameters in most of the available guidelines, the use of joint analysis of hazard and fragility can be very important, since both the reference hazard on site and the structural performance are considered. To address this issue, in the present paper, incremental dynamic analysis (IDA) was performed using 20 ground motions on four SGFs and their results were collected in the form of fragility curves. Then to obtain the annual rate of exceedance, hazard curves of the study region were generated and combined with the fragility curves, and finally, the seismic reliability of SGFs was evaluated at design basis earthquake (DBE) and maximum considered earthquake (MCE) hazard levels. Seismic reliability results indicated that the available seismic design guidelines lead to a too conservative design for SGFs, especially when they have long periods, where at the MCE hazard level, long-period SGFs with about 58% safety margin do not even experience LS performance level. The results of this study can prove useful for a more efficient design of SGFs in seismic regions.

1. Introduction

Steel gabled frame (SGF) systems are widely used for low-rise nonresidential building construction throughout the world due to having several advantages, including the ability to cover long spans, easy transfer to other spaces, low weight despite large dimensions, fast construction, recyclable and reusable, easy maintenance, welding ability, cost efficiency, etc. SGFs are constructed in single-, two-, and multi-span forms, among which the single-span ones are more common and enjoy greater applicability due to their specific advantages, including providing space for the passage of enormous vehicles such as aircrafts, creating structures with unique architecture, and having proper structural style. The initial system of SGFs in the transverse direction are usually consists of moment frames with web-tapered, I-section members with bolted end-plate moment connections to minimize the building cost through optimization of steel weight and fabrication process. The rate of change of web depth in SGF members depends on the distribution of strong-axis bending moments along their members, where they mostly have a tapered web along the entire length of the columns as well as part of the length of the rafters. In SGFs, the strong-axis bending moments in the shoulder part and partially in the ridge part is more than the middle part of the rafter. Hence, in most developed and seismically active countries such as the United States, the critical part length (with high bending moments) in SGF rafters is usually considered span/10 from the eave line, but in order to prevent the increase of mass and consequently the occurrence of strong inertial forces in the ridge, mainly the web depth is not increased and it is prismatic. For seismic design, SGFs are generally designed as an ordinary moment frame (OMF) in the United States. As an OMF, stringent seismic compactness requirements for both local and lateral-torsional buckling are not required for economic reasons [1]. Nevertheless, if non-compact or slender sections are used in SGFs, plastic hinges are unlikely to be developed due to the loosened local and lateral-torsional buckling requirements. Also, due to the special geometry of SGFs, their column bases are typically detailed as a hinge support. This prevents the bending moment from being transferred to the foundation, which in turn makes the foundations of such structures lighter and therefore economically viable.

Numerous studies were conducted on the seismic reliability of

* Corresponding author: K. N. Toosi University of Technology, Civil Engineering Department, No. 1346, Vali-Asr Street, P.O. Box. 15875-4416, 19697 Tehran, Iran.
E-mail address: fanaie@kntu.ac.ir (N. Fanaie).

https://doi.org/10.1016/j.istruc.2022.01.004
Received 23 November 2021; Received in revised form 25 December 2021; Accepted 4 January 2022
Available online 17 January 2022

various structures, including bridges [2,3], nuclear power plants [4,5], dams [6,7] and base-isolated buildings [8,9]. However, due to the fact that SGFs are considered as light structures, very few studies on their seismic reliability have been reported so far. Hence, despite the wide application of SGF systems in large industrial projects, there is a lack of knowledge regarding their seismic performance under seismic loadings. This is while despite the residential buildings with rigid diaphragm and lumped mass at roofs, this type of structure has its own specific seismic performance that should be studied. Moreover, there is still a lack of codes or standards dealing with these systems as peculiar load-carrying structures.

Several experimental and analytical studies were performed by Lee et al. [10–13] which provided design guidance and provisions for the design of the web-tapered members and developed by Forest and Murray [14], Shiomi and Kurata [15] and Ashakul and Murray [16]. Moreover, studies on the seismic behavior of SGFs consisted of web-tapered members have been conducted by several researchers. The shaking table test of 1/5 scale SGFs with compact web-tapered members was carried out by Hwang et al. [17]. The experimental results showed that if the width-thickness and depth-thickness ratios do not satisfy the requirements of the compact section, premature local buckling may occur prior to lateral buckling. The testing also revealed that the elastic flexural strains at various locations of the web-tapered members were basically identical. In inelastic tests, wide-width plastic hinges as well as small local ductility demand were observed. In another study, the LRFD strength of web-tapered members was investigated by Sumner [18] and Miller and Earls [19]. It was concluded that the LRFD shear strength provisions were overly conservative. The LRFD shear strength for web-tapered members was limited to the elastic or inelastic buckling strength of the web plate. The results also showed that development of flexural ductility in web-tapered members was difficult. Cyclic testing of full-scale SGFs consisted of non-compact built-up, web-tapered members was performed by Hong and Uang [20]. The test frame failed due to lateral-torsional buckling of the web-tapered members with significant strength degradation. The test results indicated that the system had very high deformability, but the ductility was limited. A similar conclusion was reported by Wang et al. [21]. They experimentally studied the hysteretic behavior of 1/3 scale SGFs with web-tapered members and determined the ductility coefficient of the test frame to be only 1.46. Two shaking table tests of full-scale SGFs with non-compact and slender web-tapered members, one on a specimen with light metal panel sidewalls and the other on a specimen with heavy concrete sidewalls, were conducted by Smith [22]. Each specimen consisted of two parallel identical symmetrically SGFs, and all four rafters exhibited lateral-torsional buckling near pinch points. The shaking table test of 1/3 scale SGFs consisted of non-compact built-up, web-tapered members was conducted by Su et al. [23]. The test results showed that the governing failure modes were the loosening of bolts at column bases and local buckling accompanied by lateral-torsional buckling of rafters. Besides, significant stiffness degradation in the elastic–plastic stage demonstrated that the ductility of light SGFs was limited. It should be noted that previous studies were mostly experimental and loaded by monotonic or cyclic, quasi-static loading, while the results of analytical investigations with dynamic loading as well as considering different sources of uncertainty (e.g., record to record uncertainty, etc.) are relatively lacking. Moreover, in the studies mentioned above, the entire length of the rafter members was web-tapered, which did not reflect the current construction practice. Also, the current literature lacks accurate information on seismic performance of SGFs to ensure satisfactory performance at different levels of earthquake intensity. This is while the seismic reliability evaluation of SGFs is of great importance and a key problem in regions with high seismicity, given the enormous costs of industrial equipment and the remarkable number of individuals working in these structures.

Given the scant information on the structural performance and seismic design parameters of SGFs in most of the available guidelines, the use of joint analysis of hazard and fragility can be very important since both the reference hazard on site and the structural performance are taken into account. Malekizadeh et al. [24] indicated that disregarding the hazard of the study region in the investigation of the seismic behavior of SGFs leads to a significant deviation of the outcomes from the actual results and needs to be combined with the results of structural analysis. Therefore, in the present study, the seismic reliability of four SGFs using joint analysis of hazard and fragility are investigated. The remainder of this paper is organized as follows. In section 2, details of the examined SGFs are provided in terms of geometric characteristics and design properties. In section 3, details relevant to nonlinear modeling and gravity loading of the examined SGFs are presented. In section 4, the seismic hazard of the site and selection of hazard-consistent ground motions are performed. In section 5, IDA analysis is conducted on four various SGFs and the production of fragility curves. In section 6, to obtain the annual rate of exceedance, joint analysis of hazard and fragility is performed and finally, the seismic reliability of the examined SGFs is evaluated. The results are discussed at design basis earthquake (DBE) and maximum considered earthquake (MCE) hazard levels, and some concluding remarks on the seismic reliability of SGFs are presented in section 7.

2. SGF geometry and design details

In this paper, four 2D SGF models with different spans and heights were selected to investigate their structural behavior. The geometric characteristics of SGFs are shown in Fig. 1. Also, the names and geometric dimensions of each SGF are presented in Table 1. As mentioned in the literature, the entire length of the columns as well as the region with a length of span/10 in rafters from the eave line (l_{cr}) are characterized by web-tapered members, while the rest of the length of the rafters up to the ridge is prismatic. The roof slope is considered 20% and the base of the columns enjoys hinge support. The fundamental period of SGFs is considered as a criterion for the classification of models, so that S20H6 and S60H6 as well as S20H12 and S60H12 are classified as representative of short-period SGFs and long-period SGFs in the present study, respectively. It should be mentioned that due to the greater stiffness of SGFs compared to conventional frames, such frames have a shorter period.

The density of steel is 7850 kgf/m^3. Young's modulus for steel is equal to 2.039E + 10 kgf/m^2, and the Poisson ratio is 0.3. In this study, ST37 steel was used for the rafters and columns. As mentioned in the literature, for seismic design, SGFs are generally designed as an OMF. Therefore, in all examined SGFs, OMF was incorporated as the lateral force resisting system. The modeling site of Tehran, Iran, was a region with high seismicity and with tectonic characteristics of Class D soil in line with NEHRP [25]. The gravity loads applied to the models were dead load, balanced snow load and unbalanced snow load. Walls and roofs were covered with sandwich panels with a weight of 360 kgf/m. ASCE/SEI 7–10 code [26] was deployed for gravity and lateral loading. The models were designed based on the load and resistance factor design (LRFD) method according to AISC 360–10 and AISC 341–10 codes [27,1]. According to AISC 341–10 code [1], in OMF there is no need to meet the stringent seismic compactness requirements. Nevertheless, if non-compact or slender sections are used in SGFs, plastic hinges are unlikely to be developed due to the loosened local and lateral-torsional buckling requirements. Therefore, in the present study, the compact section according to AISC 360–10 code [27] has been employed, which causes more plastic moment capacity of the members to be used before local and lateral-torsional buckling occurs. It is noteworthy that in designing 2D models, it is assumed that the distances between the fly braces (lateral-torsional braces) in the rafter and the column are 1.7 m and 2 m, respectively, and the distances between the struts (lateral braces) in the rafter and the column are 5.1 m and 3 m, respectively. After completing the design steps and by employing the trial-and-error approach to achieve an economical model, the section dimensions of

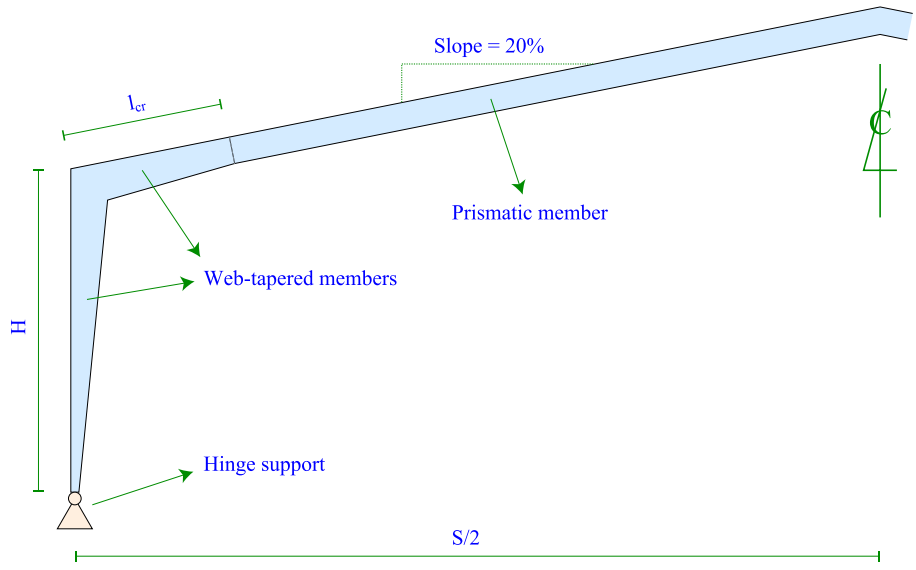

Fig. 1. Geometric characteristics of SGFs.

Table 1
Geometric dimensions of SGFs.

Model	S (m)	H (m)	l_{cr} (m)
S20H6	20	6	2
S20H12	20	12	2
S60H6	60	6	6
S60H12	60	12	6

the rafter and column members were identified, which are given in Table 2.

3. SGF nonlinear modeling and gravity loading details

The open system for earthquake engineering simulation (OpenSees) [28] is a software framework for simulating the seismic response of structural and geotechnical systems. OpenSees has been developed as a computing platform for research in performance-based earthquake engineering at the pacific earthquake engineering research center. This software has advanced capabilities for modeling and analyzing the nonlinear response of systems and seems promising as an important means of modeling and analyzing both the linear and nonlinear behaviors of structural systems. Hence, for nonlinear modeling and analyzing the SGF system, the OpenSees software, as an open-source software, was employed.

OpenSees was used in the 2D modeling of SGFs. The damping ratio was set to 5% and for modeling the viscous damping, Rayleigh damping was applied [29]. To transfer the stiffness and resisting force of the rafter elements from the basic system to the global coordinate system in a totally accurate way through geometric transformation, a corotational transformation was adopted. In the OpenSees materials library, uniaxial bilinear steel material with kinematic hardening of 0.02 entitled steel01 was selected. The fiber section was assigned to the rafter and column elements. Therefore, using defined nonlinear materials enables the nonlinearization of all the components of such sections. The nonlinear behavior of the materials in the rafters and columns was modeled using a *nonlinear beam-column element* with distributed plasticity. It should be noted that in this study, shear deformations are also considered. Due to sufficient lateral and lateral-torsional braces as well as the use of the compact section in the members of the examined SGFs, buckling is not expected to occur in the third dimension. Consequently, in the 2D models developed in OpenSees, it is not necessary to perform out-of-plane buckling modeling.

For modeling the web-tapered members of the rafters and columns, prismatic microelements with variable depth were employed and six integration points were considered for each microelement. Modeling of web-tapered members using prismatic microelements with variable depth has been adopted in the studies of Mohri et al. [30], Kucukler and Gardner [31], and Quan et al. [32], which confirms the use of this modeling method. However, for the first time, a model of SGFs with web-tapered members has been developed using prismatic microelements with variable depth on the OpenSees platform. The study of Liu et al. [33] showed that in modeling web-tapered members using prismatic microelements with variable depth, the accuracy of modeling increases with increasing the number of microelements. Therefore, in order to increase the accuracy of modeling in the mentioned method, the depth difference between the two sections of adjacent microelements (Δh_0) was considered to be a very small value, i.e., 0.02 m.

In this study, to develop the SGF model and perform gravity loading in OpenSees, the rafter member and column member were divided into two parts and one part, respectively. Each part has its own characteristics of prismatic microelements and gravity loading, i.e., Δh_0, length of microelements (l_0), number of microelements (n_0), point dead loads (P_d) and point snow loads (P_s), which are shown in Fig. 2, and their values

Table 2
Section dimensions of the rafter and column members.

Model	Column web height at top (m)	Column web height at bottom (m)	Rafter web height at ridge (m)	Rafter web height at eave (m)	Web thickness (m)	Flange thickness (m)	Flange width (m)
S20H6	0.8	0.3	0.4	0.8	0.008	0.010	0.18
S20H12	1.0	0.3	0.5	1.0	0.010	0.012	0.24
S60H6	1.5	0.3	1.0	1.5	0.014	0.018	0.34
S60H12	1.5	0.3	1.0	1.5	0.014	0.020	0.40

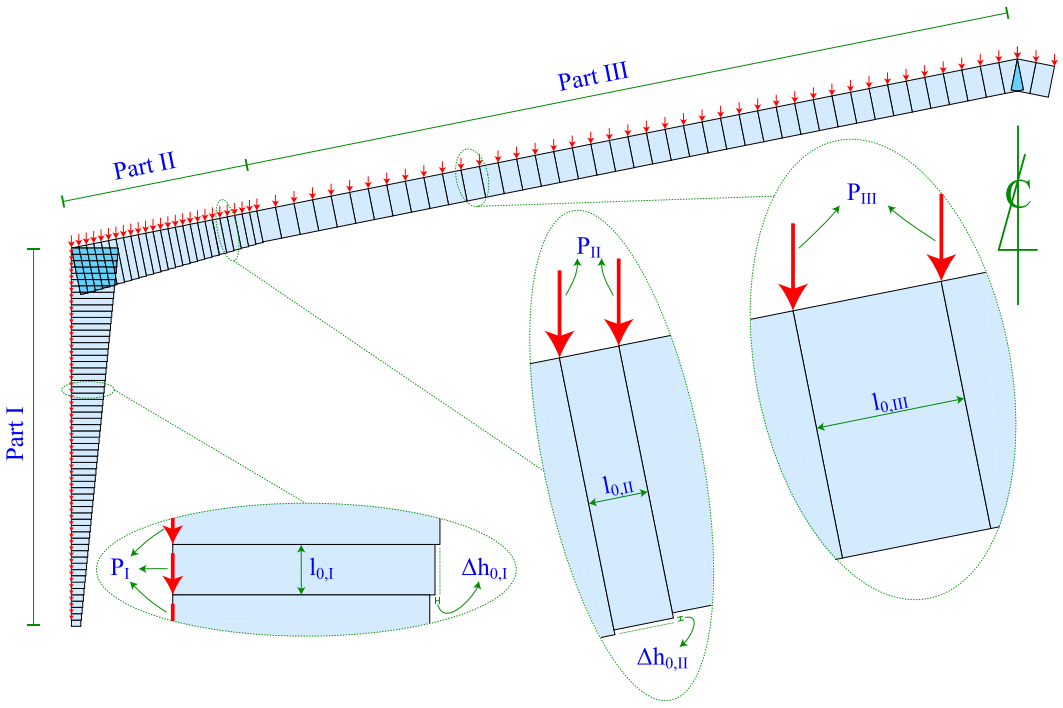

Fig. 2. Schematic representation of the SGF model developed in OpenSees.

are presented in Table 3. It is noteworthy that in Part III, microelements with a length of 2.5 $l_{0,II}$ were considered. Also, dead loads on the roofs and walls (i.e., rafters and columns) and snow loads only on the roofs (i.e., rafters) were applied concentratedly to each node according to the loading area. It should be noted that due to the greater criticality of balanced snow load than its unbalanced counterpart, the balanced snow load was used in conjunction with dead load in the gravity analysis. Fig. 3 shows the deformations created in the SGF model under gravity loads. As can be seen, due to the using prismatic microelements for modeling web-tapered members, in addition to considering displacements of the member ends (Δ), the local deformation relative to the member chord between the end nodes (δ) is also considered. Besides, under gravity loads, the rafter has double curvature and the column has single curvature. The absolute gravity drift angle ($|\Theta_g|$) in the rafter and column members for SGF models is presented in Table 4. Given that in this paper the ground motions are applied horizontally on SGF models, so despite the fact that Θ_g is higher in the rafters than in the columns, the drift angle in the column is considered as a criterion. In other words, if the vertical component of earthquake is applied to SGFs, it is necessary to check the drift angle in the rafter and column simultaneously as a criterion. After completing the nonlinear modeling process of SGFs in OpenSees, the first-mode horizontal period (fundamental period) of the structure was determined by performing an eigenvalue analysis and given in Table 5. Validation of the SGF model was presented by Malekizadeh et al. [24].

Table 3
Characteristics of prismatic microelements and gravity loading.

Model	Part	Δh_0 (m)	l_0 (m)	n_0	P_d (kgf)	P_s (kgf)
S20H6	I	0.02	0.24	2 × 25	86.4	–
	II	0.02	0.10	2 × 20	36.0	58.8
	III	–	0.25	2 × 33	90.0	147.1
S20H12	I	0.02	0.34	2 × 35	122.4	–
	II	0.02	0.08	2 × 25	28.8	47.1
	III	–	0.20	2 × 41	72.0	117.7
S60H6	I	0.02	0.10	2 × 60	36.0	–
	II	0.02	0.24	2 × 25	86.4	141.2
	III	–	0.60	2 × 41	216.0	353.0
S60H12	I	0.02	0.20	2 × 60	72.0	–
	II	0.02	0.24	2 × 25	86.4	141.2
	III	–	0.60	2 × 41	216.0	353.0

4. Seismic hazard and selection of ground motions

In this study, the hazard curves are obtained by considering the 5% damped first-mode spectral acceleration ($Sa(T_1,5\%)$) as intensity measure (IM). For the considered location of SGFs, seismic hazard is calculated using the probabilistic seismic hazard analysis (PSHA). The PSHA in this paper has been considered from the results of the Phase I project of the Greater Tehran region to a radius of 150 km [34] developed by the Engineering Optimization Research Group of the University of Tehran, Iran. Their output was presented in the form of simplified uniform hazard spectra with 5% damping with 475-year and 2475-year return periods. Therefore, a linear function is calibrated in a log–log space to match the relation between the seismic hazard and the spectral acceleration corresponding to the fundamental period of SGFs as expressed in Eq. (1) [35]:

$$\lambda_{IM}(x) = k_0 x^{-k} \tag{1}$$

Where $\lambda_{IM}(x)$ is the annual rate of IM exceeding at x, k is the log–log slope and k_0 can be thought of as the annual rate of exceeding a unit IM. To determine the hazard curve, the unknown parameters k and k_0 must be calculated. In the present study, the unknown parameters k and k_0 according to the fundamental period of SGFs were prepared from Malekizadeh et al. [24] and their values are presented in Table 6, and using simplified uniform hazard spectra with 5% damping with 475-year and 2475-year return periods for 22 different regions of Tehran located in site soil class-D (V_{S30} = 255 m/sec) were determined. Details about the seismic hazard coordinate system of 22 regions of Tehran can be found in [24].

For probabilistic seismic performance assessment, the selection of appropriate ground motions that are representatives of the seismic hazard of the site under consideration is very important. Accordingly, the ground motions used in this study were selected with tectonic characteristics of Class D soil (similar to site soil). Also, since the dynamic response of a system is highly dependent on the earthquake

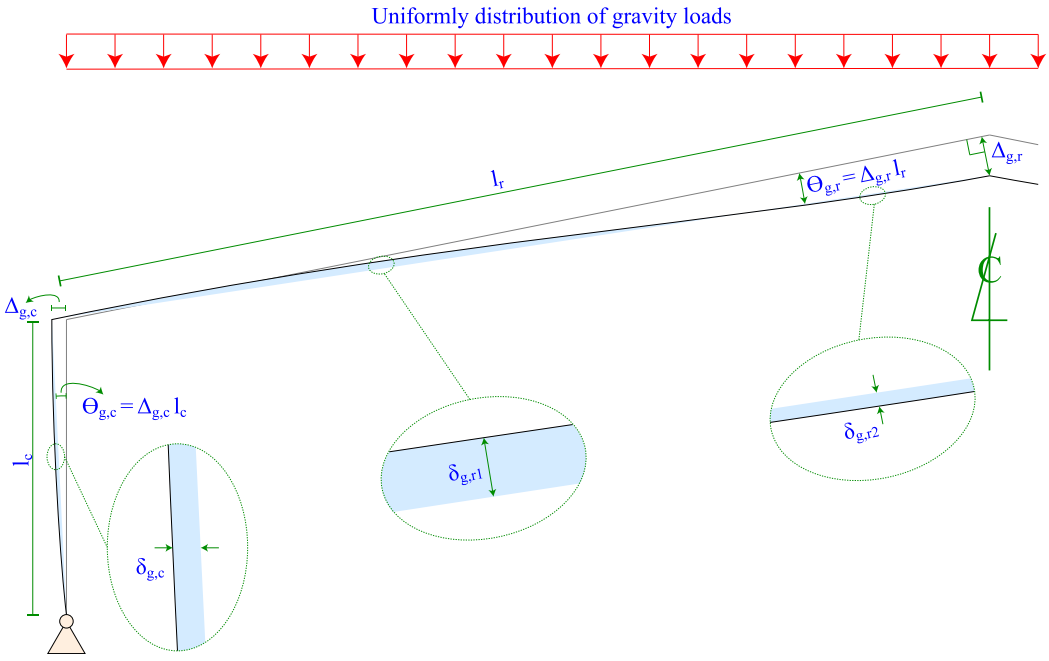

Fig. 3. Deformations created in the SGF model under gravity loads.

Table 4
Absolute gravity drift angle in the rafter and column members.

Model	member	$\lvert\Theta_g\rvert$ (rad)
S20H6	Rafter	0.00734
	Column	0.00246
S20H12	Rafter	0.00434
	Column	0.00073
S60H6	Rafter	0.00527
	Column	0.00511
S60H12	Rafter	0.00795
	Column	0.00402

Table 5
Fundamental period of SGF models.

Model	Fundamental period (sec)
S20H6	0.90
S20H12	1.53
S60H6	0.63
S60H12	1.31

Table 6
Hazard curve parameters [24].

Model	k	k_0
S20H6	2.421	32.683E-05
S20H12	2.408	4.350E-05
S60H6	2.437	79.344E-05
S60H12	2.416	8.066E-05

records, an appropriate number of ground motions must be selected to cover the response range of the structure. According to Shome and Cornell [36], the use of 10 to 20 ground motions often leads to acceptable accuracy in damage demand estimation. Hence, in the present study, 20 ground motions in FEMA P695 [37] were selected from the PEER-NGA database [38] for nonlinear dynamic analyses. This set covers a wide range of moment magnitude (M_W) between 6.54 and 7.62, and the closest distance from the recording site to the ruptured area (R_{rup}) is up to about 23 km. Also, from each ground motion, a horizontal component with more PGA was used. Details of the selected ground motions are provided in Table 7, where their elastic response spectrum was generated by Seismosignal software [39].

5. IDA analysis and production of fragility curves

As mentioned in the literature, since SGFs are very sensitive to the formation of plastic hinges, it is necessary to evaluate their behavior in the nonlinear region, and it seems that using of incremental dynamic analysis (IDA), which includes a large number of nonlinear time-history analyses under a set of ground motions, is a suitable option for them. Therefore, considering that the major goal of this paper is the seismic reliability evaluation of SGFs at different levels of earthquake intensity, IDA analysis was performed using the 20 ground motions selected in section 4, and the multi-record IDA curves for the examined SGFs are revealed in Fig. 4. Prior research [24] has clearly indicated that in the probabilistic seismic assessment of SGFs, the use of Sa(T_1,5%) and the absolute maximum drift angle ($\Theta_{a,max}$) as IM and damage measure (DM),

Table 7
Selected ground motions.

No.	Event	Station	M_w	PGA_{max} (g)
1	Chi-Chi Taiwan	CHY101	7.62	0.340
2		TCU065	7.62	0.575
3	Duzce Turkey	Bolu	7.14	0.806
4		Duzce	7.14	0.515
5	Erzican Turkey	Erzincan	6.69	0.496
6	Imperial Valley-06	Bonds Corner	6.53	0.777
7		Chihuahua	6.53	0.254
8		Delta	6.53	0.350
9		El Centro Array #6	6.53	0.449
10		El Centro Array #7	6.53	0.469
11		El Centro Array #11	6.53	0.367
12	Kobe Japan	Shin-Osaka	6.90	0.233
13	Kocaeli Turkey	Yarimca	7.51	0.322
14	Loma Prieta	Capitola	6.93	0.439
15		Gilroy Array #3	6.93	0.368
16	Northridge-01	Beverly Hills-Mulhol	6.69	0.488
17		Canyon-W Lost Cany	6.69	0.404
18		Rinaldi Receiving Sta	6.69	0.472
19	San Fernando	LA-Hollywood Stor FF	6.61	0.195
20	Superstition Hills	El Centro Imp. Co. Cent	6.54	0.357

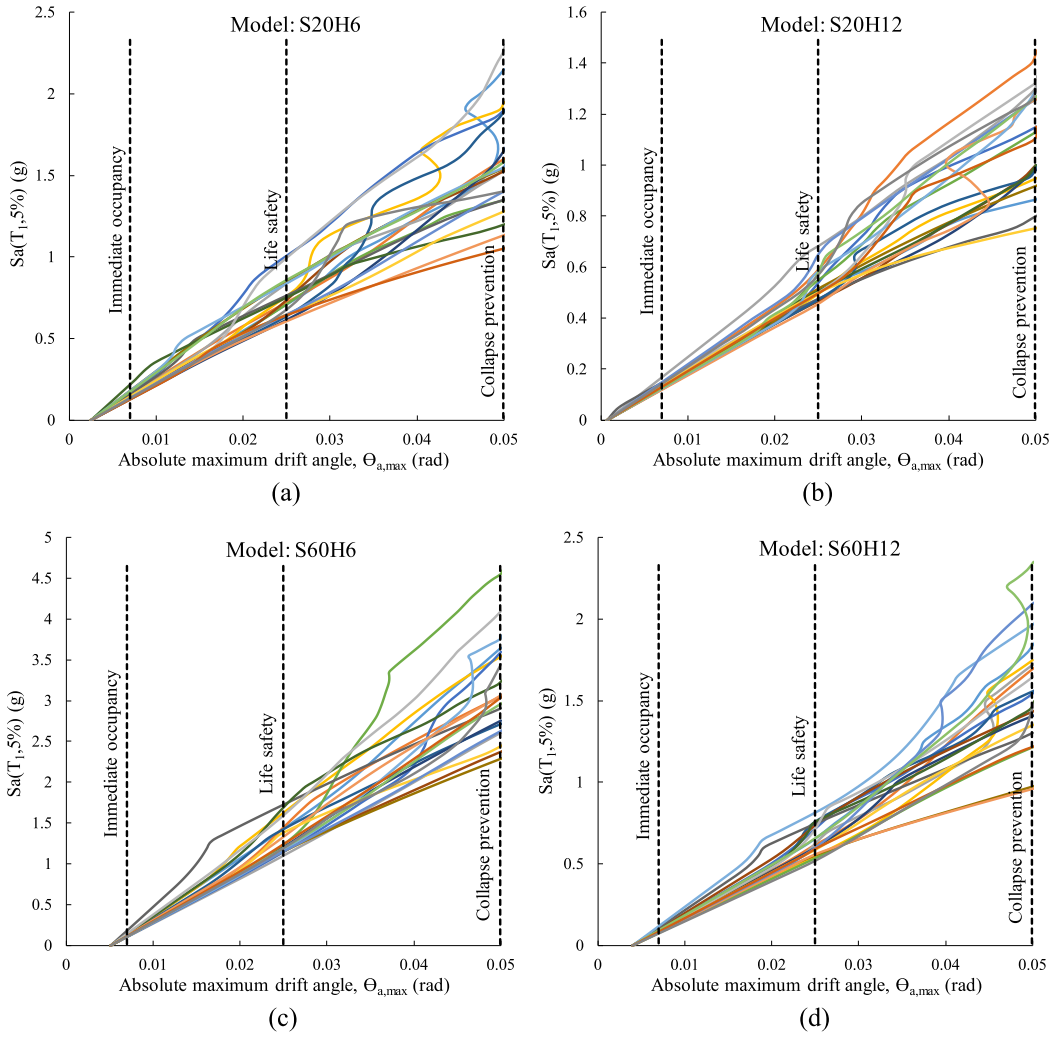

Fig. 4. Multi-record IDA curves for (a) S20H6, (b) S20H12, (c) S60H6, and (d) S60H12.

respectively, led to a very strong correlation between IM and DM. Therefore, since in section 4 Sa(T_1,5%) was selected as IM, here, $\Theta_{a,max}$ was considered as DM. As explained in section 3, since in this paper the ground motions were applied horizontally to the SGF models, $\Theta_{a,max}$ in the columns was considered as a criterion. The scale factor of ground motions was defined as a multiplication of Sa(T_1,5%) from a very low

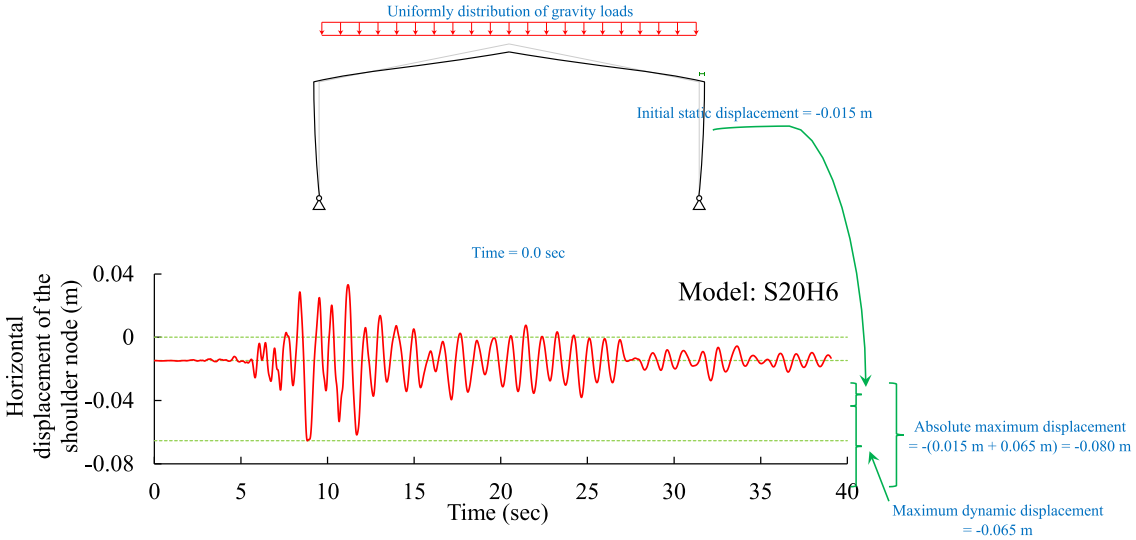

Fig. 5. Horizontal displacement time-history curve corresponding to the shoulder node for S20H6.

level with incremental steps of 0.05 g to a high level where the collapse of the structure occurs, and the $\Theta_{a,max}$ parameter was recorded at each step of the analysis. According to FEMA 356 [40], three performance levels of immediate occupancy (IO), life safety (LS) and collapse prevention (CP) were considered as damage levels with the $\Theta_{a,max}$ values of 0.7, 2.5 and 5%, respectively. It is noteworthy that due to insufficient information of the regulations on the performance-based design of SGF systems, in the FEMA 356 [40], conventional steel frame systems were used to determine the performance levels of DM. It should be noted that before conducting the nonlinear time-history analysis at each step of the IDA analysis, static analysis was performed under gravity loads. Because of the specific geometrical characteristics of SGFs (sloping rafters), gravity loads create an initial horizontal displacement in the shoulder. In addition, the hinge supports amplify the mentioned horizontal displacement, as can be clearly seen in Fig. 4. Therefore, SFGs experience a static displacement in the initial state due to gravity loads. After incorporating the ground motion, the absolute maximum displacement for SFGs involves initial static displacement resulting from the gravity loads plus maximum dynamic displacement resulting from the ground motion. For example, in Fig. 5, results of the nonlinear time-history analysis for S20H6 using the Imperial Valley-06 earthquake record at the El Centro Array #11 station with a peak ground acceleration (PGA) of 0.367g are provided in the form of horizontal displacement time-history curves corresponding to the shoulder node. It is noteworthy that $\Theta_{a,max}$ is an absolute value so it appears positive in IDA curves.

In order to derive the conditional probability of reaching a certain damage level for a given IM from the outputs of IDA analysis, diagrams called fragility curves are used. Using the results of IDA analysis and the performance levels corresponding to various damage levels, it is now possible to generate fragilities by Eq. (2) [41]:

$$\boldsymbol{P(DM|IM) = P[DM > y|IM = x]} \tag{2}$$

Where $P\,[DM > y \mid IM = x]$ defines the probability of DM exceeding the value y given that IM equals x.

Assuming a lognormal distribution for DM given IM, Eq. (2) is rewritten as a closed form in the following [42]:

$$\begin{aligned}&\boldsymbol{P[DM > y|IM = x]}\\&= 1 - \boldsymbol{P[DM < y|IM = x]}\\&= 1 - \Phi\left(\frac{\boldsymbol{\ln y - \ln \eta(x)}}{\boldsymbol{\beta}}\right)\\&= \Phi\left(\frac{\boldsymbol{\ln \eta(x) - \ln y}}{\boldsymbol{\beta}}\right)\end{aligned} \tag{3}$$

Where $\eta(x)$ and β are the logarithmic mean and logarithmic standard deviation of DM given IM, respectively, and are obtained using the results of IDA analysis and the power law function [43]. $\Phi(.)$ is the cumulative function of standard normal distribution.

Fragility curves are developed for various SGFs using the closed form of fragility function shown in Eq. (3). Plots of the fragility curves for SGFs with $\Theta_{a,max}$ as the DM are shown in Fig. 6, which illustrate the relative vulnerability of the four SGFs over a range of earthquake intensities and damage levels. The relative vulnerability of various SGFs is compared in terms of their probability of entering into different damage levels. Fragility curves for various SGFs are also compared by evaluating the relative change in the median value of the fragility curves.

The evaluation of the fragility curves offered a valuable insight on the seismic performance of various SGFs in terms of the probability of damage. From Fig. 6a it is evident that all SGFs have the similar probability of damage irrespective of the intensity level. However, the probability of damage for various SGFs is more pronounced in the other damage levels. According to Fig. 6b, in general, S60H6 shows better seismic performance at CP performance level as compared to other models. As depicted in Fig. 6c, S20H12 is more likely to experience damage at a lower intensity while S60H6 showed much better performance as it showed only 12% probability of damage at a Sa(T_1,5%) of 3 g. However, an interesting behavior is observed at all performance levels where S20H12 and S60H12 (long-period SGFs) have the highest probability of damage and S60H6 and S20H6 (short-period SGFs) have the lowest one.

The various SGFs are also compared in terms of the relative change in the median value of the fragility curves which indicates the Sa(T_1,5%) associated with a 50% probability of reaching a certain performance level. Table 8 compares the median Sa(T_1,5%) for different performance levels of four various SGFs. The median Sa(T_1,5%) for various SGFs at IO performance level ranges from 0.09 g to 0.15 g. However, at higher performance levels, i.e., at LS and CP, the median Sa(T_1,5%) varies over a wide range from 0.54 g to 1.23 g and 1.18 g–3.94 g for LS and CP, respectively.

As mentioned above, at the IO performance level, similar behavior of SGFs seismic performance was observed, which can be due to the initial gravity drift angle that causes SGFs to experience this performance level at very low earthquake intensities. As a result, accurate seismic dynamic behavior of SGFs cannot be observed at the IO performance level. $\Theta_{a,max}$ due to primary static gravity loads and secondary dynamic seismic loads relative to the IO performance level for various SGFs are shown in Fig. 7. The highest $\Theta_{a,max}$ due to gravity loads relative to the IO performance

Table 8
Comparison of median Sa(T_1,5%) (g).

Model	IO	LS	CP
S20H6	0.140	0.740	1.835
S20H12	0.127	0.539	1.184
S60H6	0.146	1.231	3.935
S60H12	0.091	0.617	1.751

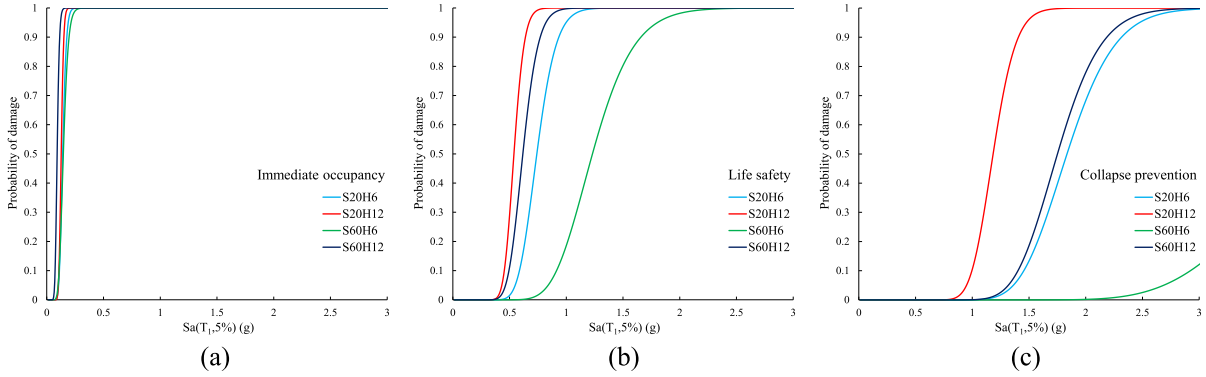

Fig. 6. Fragility curves at (a) IO, (b) LS, and (c) CP performance levels.

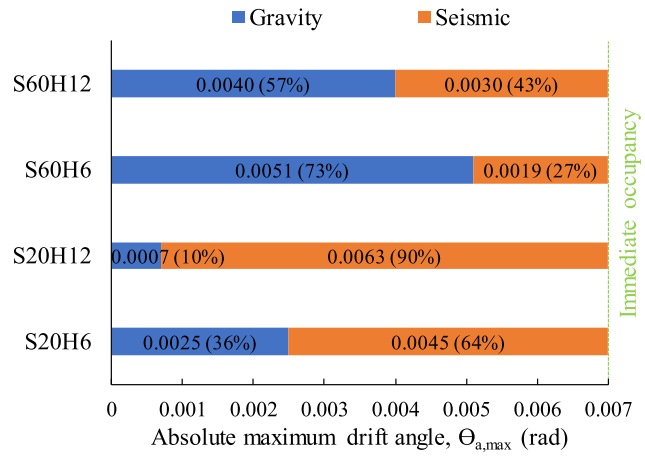

Fig. 7. $\Theta_{a,max}$ due to primary static gravity loads and secondary dynamic seismic loads relative to the IO performance level.

level for S60H6 and S60H12 are 73% and 57%, respectively, and the lowest one for S20H12 and S20H6 are 10% and 36%, respectively. However, S60H6, which has the shortest period among the models, although requires only 19% $\Theta_{a,max}$ due to seismic loads to reach the IO performance level, it needs the most earthquake intensity (i.e., 0.15 g) compared to other models to experience this performance level. On the other hand, S20H12, which has the longest period among the models, requires 90% $\Theta_{a,max}$ due to seismic loads to reach the IO performance level but experiences this performance level at low earthquake intensity (i.e., 0.13 g).

6. Joint analysis and SGF seismic reliability

Joint analysis of hazard and fragility is becoming an extensive and unavoidable tool for estimating earthquake casualties. Given the scant information on the seismic performance of steel gabled frames (SGFs) with web-tapered members in most of the available seismic design guidelines, the use of such an analysis can be very important since both the reference hazard on site and the structural performance are considered. Joint analysis of hazard and fragility in terms of the annual rate of DM exceeding is expressed as Eq. (4) [41]:

$$\lambda_{DM}(y) = \int \overbrace{P[DM > y|IM = x]}^{Fragility} \left| \overbrace{d\lambda_{IM}(x)}^{Hazard} \right| \tag{4}$$

Eq. (4) consists of two terms of hazard and fragility, which were estimated in sections 4 and 5, respectively. The annual rate of exceeding different damage levels is developed for various SGFs by combining the results of hazard and fragility according to Eq. (4). Then the return period and the probability of exceedance in 50 years corresponding to performance levels were obtained, which are listed in Table 9. Results show that all SGFs have a very high probability of IO (probability of exceeding IO performance level in 50 years) while S60H6 has the highest probability of 500%, which is 58%, 93% and 71% higher than of S20H6, S20H12 and S60H12, respectively. A comparison of the four SGFs in terms of exceeding LS reveals that S20H12 has the lowest probability of exceeding LS performance level in 50 years, which is only 1.02%. On the other hand, S20H6 resulted in the highest probability of exceeding LS performance level in 50 years, which is 3.73%. Also, all SGFs have a low probability of CP, which S60H12 has the lowest probability of 0.11%. Among the four various SGFs, S20H6 has the highest probability of CP, which is 63%, 56% and 73% higher than S20H12, S60H6 and S60H12, respectively. However, an interesting behavior is observed at all performance levels where S60H6 and S20H6 (short-period SGFs) have the highest annual probability of exceedance and S20H12 and S60H12 (long-period SGFs) have the lowest one. A closer look into the probability of damage and the annual probability of exceedance for various SGFs presented in sections 5 and 6, respectively, shows that the annual rate is strongly influenced by the seismic hazard of the site. Where without incorporating the seismic hazard, short-period SGFs had better seismic performance than long-period SGFs, but after integrating the seismic hazard with the results of fragility analysis, the outcomes were completely reversed so that short-period SGFs had a higher annual rate than long-period SGFs.

Table 9
Annual rate, return period and probability of exceedance in 50 years corresponding to performance levels.

Model	Performance levels	Annual rate of exceedance	Return period (year)	Probability of exceedance in 50 years (%)
S20H6	IO	4.21E-02	24	208.33
	LS	7.45E-04	1342	3.73
	CP	8.28E-05	12,077	0.41
S20H12	IO	0.66E-02	151	33.11
	LS	2.03E-04	4917	1.02
	CP	3.05E-05	32,758	0.15
S60H6	IO	10.21E-02	10	500.00
	LS	5.62E-04	1781	2.81
	CP	3.30E-05	30,269	0.17
S60H12	IO	2.89E-02	35	142.86
	LS	2.83E-04	3538	1.41
	CP	2.27E-05	43,966	0.11

Herein, a basic safety objective (BSO) in accordance with FEMA 356 [40] has been used to evaluate the seismic reliability of various SGFs. The BSO is intended to approximate the earthquake risk to life safety traditionally considered acceptable in the United States. Buildings meeting the BSO are expected to experience little damage from relatively frequent and moderate earthquakes, but significantly more damage and potential economic loss from the most severe and infrequent earthquakes that could affect them. The level of damage and potential economic loss experienced by buildings rehabilitated to the BSO may be greater than that expected in properly designed and constructed new buildings. Therefore, the buildings when subjected to design basis earthquake (DBE) and maximum considered earthquake (MCE) hazard levels should not exceed LS and CP performance levels, respectively. As mentioned earlier, due to insufficient information of the regulations on the performance-based design of SGF systems, in the FEMA 356 [40], conventional steel frame systems were used. Fig. 8 illustrates the seismic reliability of four various SGFs in terms of $\Theta_{a,max}$ hazard and safety at the DBE (return period = 475 years) and MCE (return period = 2475 years) hazard levels relative to the LS and CP performance levels, respectively. At the DBE hazard level, the highest $\Theta_{a,max}$ hazard relative to the LS performance level for S60H6 and S20H6 are similarly 72%, and the lowest one for S20H12 and S60H12 are 42% and 58%, respectively. In other words, all SGFs subjected to DBE are between the IO and LS performance levels, indicating that the available seismic design guidelines lead to an acceptable design for SGFs. However, S20H12 and S60H12, which are in the category of long-period SGFs, appear to be too conservative with 57% and 42% $\Theta_{a,max}$ safety, respectively. On the other hand, at the MCE hazard level, the situation is similar to the DBE hazard level, except that short-period SGFs subjected to MCE are between the LS and CP performance levels with about 43% $\Theta_{a,max}$ safety. However, long-period SGFs subjected to MCE do not experience the LS performance level, where they appear to be very conservative with about 58% $\Theta_{a,max}$ safety. A closer look reveals that under more severe earthquakes, $\Theta_{a,max}$ safety increases, and the available seismic design guidelines lead to a more conservative design.

7. Conclusion

In this study, IDA analysis was performed using 20 ground motions on four SGFs, and their results were collected in the form of fragility

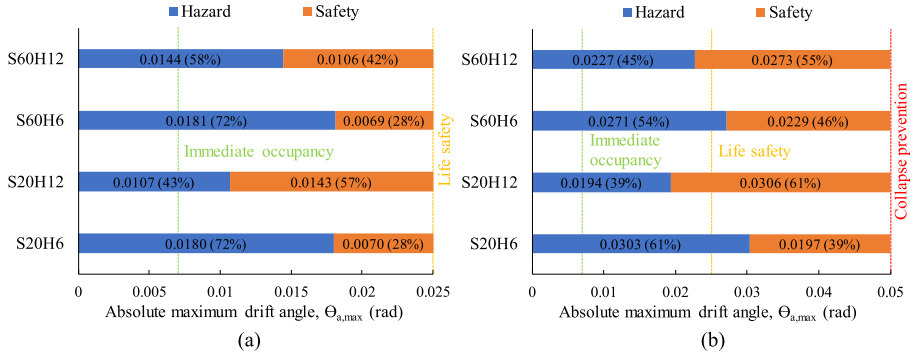

Fig. 8. $\Theta_{a,max}$ hazard and safety at (a) DBE, and (b) MCE hazard levels relative to the LS and CP performance levels, respectively.

curves. Then to obtain the annual rate of exceedance, hazard curves of the study region were generated and combined with the fragility curves, and finally, the seismic reliability of SGFs was evaluated at DBE and MCE hazard levels. Some of the main findings as the contributions of the present research are as follows:

- From Fig. 7, it can be concluded that the geometric dimensions of SGFs are an important factor in the amount of $\Theta_{a,max}$ due to gravity loads, but for $\Theta_{a,max}$ due to seismic loads, the fundamental period of SGFs is the determining criterion. The results of the primary static gravity analysis clearly showed that the S60H6 and S60H12, which are in the category of long-span SGFs, experienced more $\Theta_{a,max}$ due to gravity loads than S20H6 and S20H12, which are in the category of short-span SGFs. But the results of the secondary dynamic seismic analysis revealed that the S60H12 and S20H12, which are in the category of long-period SGFs, experienced more $\Theta_{a,max}$ due to seismic loads compared to S60H6 and S20H6, which are in the category of short-period SGFs.
- The initial drift angle due to gravity loads caused SGFs to experience the IO performance level under very low earthquake intensity, especially when they had short periods. The S60H6, which has the shortest period among other models, had the highest probability of exceeding IO performance level in 50 years by 500%. This means that the seismic behavior evaluation of SGFs at the IO performance level cannot be important. Therefore, it is recommended that if the performance levels of FEMA 356 are used for the seismic behavior evaluation of SGFs, the IO performance level can be ignored.
- In general, the results of fragility analysis showed that the probability of damage for long-period SGFs was higher than short-period SGFs. However, after combining fragility and hazard, the outputs demonstrated that the annual probability of damage for short-period SGFs was higher than long-period SGFs. The results of fragility analysis and joint analysis are opposite. This is due to the fact that in the seismic hazard curves, the annual rate values decrease with increasing the fundamental period of SGFs. Therefore, in the seismic behavior evaluation of SGFs, the use of fragility analysis alone is not sufficient, and it is recommended that the seismic hazard uncertainty of the site be considered. This conclusion supports the results of Malekizadeh et al. [24] on the role of seismic hazard on the seismic performance of SGFs.
- The results of seismic reliability of SGFs showed that at the DBE hazard level, the highest $\Theta_{a,max}$ hazard relative to the LS performance level for short-period SGFs was about 72%, and the lowest one for long-period SGFs was about 50%. In other words, all SGFs subjected to DBE were between the IO and LS performance levels, indicating that the available seismic design guidelines lead to an acceptable design for SGFs. However, long-period SGFs with about 50% safety margin appear to be too conservative. On the other hand, at the MCE hazard level, the situation was similar to the DBE hazard level, except that short-period SGFs subjected to MCE were between the LS and CP performance levels with about 43% safety margin. However, long-period SGFs subjected to MCE did not even experience the LS performance level, where they appear to be very conservative with about 58% safety margin. A closer look reveals that under more severe earthquakes, safety margin increases, and the available seismic design guidelines lead to a more conservative design.
- From the joint analysis of hazard and fragility for various SGFs, it is expected that the SGFs will incur a low annual loss and provide significant financial benefit in the long run since these systems showed a very low annual probability of collapse. However, a detailed loss estimation needs to be carried out before highlighting the potential financial benefit of SGFs. Moreover, performing further study considering the construction, repair and maintenance cost of SGFs, along with the development of a loss-hazard relationship, will shed more light on the potential economic benefit of this system.

Declaration of Competing Interest

The authors declare that they have no known competing financial interests or personal relationships that could have appeared to influence the work reported in this paper.

References

[1] AISC 341–10. Seismic provisions for structural steel buildings. American Institute of Steel Construction. Chicago, Illinois, USA; 2010.
[2] Chen Z-Q, Zheng S-X, Zhang J, Jia H. Seismic reliability analysis of high-pier railway bridges with correlated random parameters via an improved maximum entropy method. Structures 2021;33:4538–55. https://doi.org/10.1016/j.istruc.2021.07.039.
[3] Barmi AM, Khansefid A, Khaloo A, et al. Seismic risk assessment of optimally designed highway bridge isolated by ordinary unbounded elastomeric bearings. Numerical Methods in Civil Engineering 2021;6(1):10–21. http://nmce.kntu.ac.ir/article-1-360-en.html.
[4] Xu B, Zhou Y, Pang R. Seismic stability reliability assessment of nuclear power plant's bank revetment considering unreinforced and reinforced situations. Ann Nucl Energy 2020;136:107025. https://doi.org/10.1016/j.anucene.2019.107025.
[5] Zhou Y, Jing M, Pang R, Xu B, Jiang F, Yu X. Stochastic dynamic response and seismic reliability analysis of nuclear power plant's vertical retaining wall based on plastic failure. Structures 2021;31:513–39. https://doi.org/10.1016/j.istruc.2021.02.012.
[6] Pang R, Xu B, Kong X, Zou D, Zhou Y. Seismic reliability assessment of earth-rockfill dam slopes considering strain-softening of rockfill based on generalized probability density evolution method. Soil Dyn Earthquake Eng 2018;107:96–107. https://doi.org/10.1016/j.soildyn.2018.01.020.
[7] Chen J, Jia Q, Xu Q, Fan S, Liu P. The PDEM-based time-varying dynamic reliability analysis method for a concrete dam subjected to earthquake. Structures 2021;33:2964–73. https://doi.org/10.1016/j.istruc.2021.06.036.
[8] Shao B, Mahin SA, Zayas V. Achieving targeted levels of reliability for low-rise seismically isolated structures. Soil Dyn Earthquake Eng 2019;125:105744. https://doi.org/10.1016/j.soildyn.2019.105744.
[9] Wang N, Huang X. Global damage model for the seismic reliability analysis of a base-isolated structure. Structures 2021;34:4892–907. https://doi.org/10.1016/j.istruc.2021.10.059.
[10] Lee GC, Ketter RL, Morrell ML. Design of tapered members. Welding Research Council Bulletin, No. 173, New York, USA; 1972.
[11] Lee GC, Morrell ML. Application of AISC design provisions for tapered members. Engineering Journal, AISC 1975;12(1):1–13.

[12] Lee GC, Chen YC, Hsu TL. Allowable axial stress of restrained multi-segment, tapered roof girders. Welding Research Council Bulletin, No. 248, New York, USA; 1979.
[13] Lee GC, Hsu TL. Tapered columns with unequal flanges. Welding Research Council Bulletin, No. 272, New York, USA; 1981.
[14] Forest R, Murray TM. Rigid frame studies. Report No. FSEL/STAR 82–01. University of Oklahoma, Norman, USA; 1982.
[15] Shiomi H, Kurata M. Strength formula for tapered beam-columns. J Struct Eng 1984;110(7):1630–43. https://doi.org/10.1061/(ASCE)0733-9445(1984)110:7(1630).
[16] Ashakul A, Murray TM. LRFD versus ASD frame design study. Report No. Blacksburg, USA: Virginia Polytechnic Institute and State University; 2002.
[17] Hwang JS, Chang KC, Lee GC. Seismic behavior of gable frame consisting of tapered members. J Struct Eng 1991;117(3):808–21. https://doi.org/10.1061/(ASCE)0733-9445(1991)117:3(808).
[18] Sumner EA. Experimental and analytical investigation of the LRFD strength of web-tapered members. Blacksburg, USA: Virginia Polytechnic Institute and State University; 1995. Master thesis.
[19] Miller BS, Earls CJ. On moment capacity and flexural ductility in doubly symmetric web-tapered I-girders. Engineering Journal, AISC 2005;42:123–41.
[20] Hong JK, Uang CM. Cyclic testing of a metal building moment frame system with web-tapered members. J Constr Steel Res 2012;70:248–55. https://doi.org/10.1016/j.jcsr.2011.09.005.
[21] Wang ZS, Su MZ, Li QC, et al. Pseudo-static experimental study of a single-story single-bay light-weight portal frame with tapered members. China Civil Engineering Journal 2012;45(7):24–30. in Chinese.
[22] Smith MD. Seismic testing and analytical studies for the development of new seismic force resisting systems for metal buildings. San Diego, USA: University of California; 2013. Ph.D. dissertation.
[23] Su M, Wang H, Wang Z, Wang F. Shaking table tests on steel portal frames consisting of non-compact tapered members. J Constr Steel Res 2017;128:473–82. https://doi.org/10.1016/j.jcsr.2016.09.009.
[24] Malekizadeh M, Fanaie N, Pirasteh AA. Probabilistic seismic assessment of steel gabled frames with web-tapered members under near-fault ground motions along strike-normal and strike-parallel components. Structures 2021;34:4142–57. https://doi.org/10.1016/j.istruc.2021.10.007.
[25] NEHRP. Recommended provisions for seismic regulations for new buildings. Building Seismic Safety Council. Washington DC, USA; 2000.
[26] ASCE/SEI 7–10. Minimum design loads and associated criteria for buildings and other structures. American Society of Civil Engineers in partnership with Structural Engineering Institute. Reston, Virginia, USA; 2010.
[27] AISC 360–10. Specification for structural steel buildings. American Institute of Steel Construction. Chicago, Illinois, USA; 2010.
[28] OpenSees. Open System for Earthquake Engineering Simulation. Pacific Earthquake Engineering Research Center. University of California, Berkeley, California, USA; 2018.
[29] Chopra AK. Dynamics of structures: theory and applications to earthquake engineering. Englewood Cliffs, New Jersey, USA: Prentice-Hall; 2007.
[30] Mohri F, Meftah SA, Damil N. A large torsion beam finite element model for tapered thin-walled open cross sections beams. Eng Struct 2015;99:132–48. https://doi.org/10.1016/j.engstruct.2015.04.039.
[31] Kucukler M, Gardner L. Design of laterally restrained web-tapered steel structures through a stiffness reduction method. J Constr Steel Res 2018;141:63–76. https://doi.org/10.1016/j.jcsr.2017.11.014.
[32] Quan C, Kucukler M, Gardner L. Design of web-tapered steel I-section members by second-order inelastic analysis with strain limits. Eng Struct 2020;224:111242. https://doi.org/10.1016/j.engstruct.2020.111242.
[33] Liu SW, Bai R, Chan SL. Second-order analysis of non-prismatic steel members by tapered beam-column elements. Structures 2016;6:108–18. https://doi.org/10.1016/j.istruc.2016.02.006.
[34] Gholipoor Y, Bozorgnia Y, Rahnama M, et al. Probabilistic seismic hazard analysis phase I Tehran regions final report. Tehran, Iran: Engineering Optimization Research Group. University of Tehran; 2009. https://iranhazard.mporg.ir/.
[35] Luco N. Probabilistic seismic demand analysis, SMRF connection fractures, and near-source effects. Stanford, California, USA: University of California; 2002. Ph.D. dissertation.
[36] Shome N, Cornell CA. Probabilistic seismic demand analysis of nonlinear structures. Report No. RMS-35. Stanford University, California, USA; 1999.
[37] FEMA P695. Quantification of building seismic performance factors. Federal Emergency Management Agency. Washington DC, USA; 2009.
[38] Database P-E-E-R-N-G-A. Pacific Earthquake Engineering Research Center. Berkeley, California, USA: University of California; 2006.
[39] Antoniou S, Pinho R, Bianchi F. SeismoSignal. Version 3.2.0. 2008.
[40] FEMA 356. Prestandard and commentary for the seismic rehabilitation of buildings. Federal Emergency Management Agency. Washington DC, USA; 2000.
[41] Deierlein GG, Krawinkler H, Cornell CA. A framework for performance-based earthquake engineering. In: Pacific Conference on Earthquake Engineering. Christchurch, New Zealand; 2003.
[42] Tagawa H, MacRae G, Lowes L. Probabilistic evaluation of seismic performance of 3-story 3D one- and two-way steel moment-frame structures. Earthquake Eng Struct Dyn 2008;37(5):681–96. https://doi.org/10.1002/eqe.778.
[43] Cornell CA, Jalayer F, Hamburger RO, et al. Probabilistic basis for 2000 SAC federal emergency management agency steel moment frame guidelines. Journal of Structural Engineering 2002;128(4):526–32. https://doi.org/10.1061/(ASCE)0733-9445(2002)128:4(526).